Automated Malignancy Detection in Breast Histopathological Images

Andrei Chekkoury[1], Parmeshwar Khurd[1], Jie Ni[1], Claus Bahlmann[1], Ali Kamen[1], Amar Patel[1], Leo Grady[1], Maneesh Singh[1], Martin Groher[3], Nassir Navab[3], Elizabeth Krupinski[2], Jeffrey Johnson[1], Anna Graham[2], Ronald Weinstein[2]

[1]Siemens Corporate Research, 755 College Road East, Princeton NJ, 08540, United States;
[2]The University of Arizona, Tucson AZ 85721, United States
[3]Chair for Computer Aided Medical Procedures, Technical University of Munich, Germany

ABSTRACT

Detection of malignancy from histopathological images of breast cancer is a labor-intensive and error-prone process. To streamline this process, we present an efficient Computer Aided Diagnostic system that can differentiate between cancerous and non-cancerous $H\&E$ (hemotoxylin&eosin) biopsy samples. Our system uses *novel* textural, topological and morphometric features taking advantage of the special patterns of the nuclei cells in breast cancer histopathological images. We use a Support Vector Machine classifier on these features to diagnose malignancy. In conjunction with the maximum relevance - minimum redundancy feature selection technique, we obtain high sensitivity and specificity. We have also investigated the effect of image compression on classification performance.

Keywords: Breast histopathology, CAD histology, breast cancer, detecting malignancy, cancer in histopathology images

1. INTRODUCTION

The histopathological diagnosis is the foundation of modern oncology, and plays a major role in the treatment of many other types of disease. Errors in these reports can critically affect patient care and may become the subject of media concern. Analogous to the role of computer-assisted diagnosis (CAD) algorithms in radiological imaging, our proposed approach aims at complementing the specialized opinion of the pathologist, by using an objective judgement, making use of quantitative measures. We aim at using the proposed system in distinguishing between malignant and benign breast cancer samples, based on specially designed textural, topological and morphometric features that can capture representative structures in cancer tissue. Although we are focused on the malignancy detection problem, we note that pathologists go beyond this and report grades of malignancy

2. METHODS

Our CAD system for breast cancer malignancy detection is composed of three different steps: 1) image processing 2) feature extraction to quantify the properties of these areas, 3) classification of the relevant areas as malignant or not. In this study, we are focused on expanding the second and third steps, i.e., feature extraction and classification to find hallmarks of cancer, but we will introduce a short description of the method used for preprocessing. Breast cancer is captured using morphometrical, textural or topological features. Along similar lines, our approach uses the network cycle feature framework developed in Khurd et al. [13] and the texton-based approach described in Khurd et al. [12] as the basis for our work. We now describe the different categories of features explored in this study, which are later fed to an SVM classifier after a feature selection procedure.

2.1 Pre-processing

In Hematoxylin&Eosin (H&E) images, a special staining is performed in order to enhance specific structures. Hematoxylin is a blue dye that binds to the nuclear chromatin and eosin is an acidic pink dye that binds to the cytoplasmic structures and blood cells. Depending on the application, a separation of these dyes is helpful. Also since current imaging techniques provide very high resolution output, pre-processing these images will reduce the computational cost. The H&E separation is performed based on the method presented in Cosatto et al. [5]: the image is converted from RGB color space into the CMY color space for a better separation of the components and the two vectors corresponding to H and E are obtained.

2.2 Morphometric Features

Designed morphometric features, capture the variation in nuclei size and shape, considered as one of the most important aspects taken into consideration by pathologists [3]. We have investigated three aspects that capture morphometric features: information extracted from the Hessian matrix, information provided by the Fourier Shape Descriptors and a special designed feature, encoding the spatial arrangement of nuclei surrounding a ductal structure.

Nuclei Detection Extracting characteristic features from nuclei size and shape, requires a good nuclei detection. Extracting a precise location of nuclei plays an important role in detecting cancer in histopathology of breast cancer. Based on the work presented in Loy and Zelinsky [14], in Singh et al. [17] the fast radial symmetry has been modified and adapted in order to fit the purpose of detecting nuclei in histopathology slides.

Nuclei Segmentation is based on an improved random walker segmentation algorithm based on a previous accurate detection of nuclei. The Random Walker (RW), introduced by Grady [8], is a segmentation algorithm that captures weak or missing boundaries, but is also able to cope with noise in the image, identifying multiple objects simultaneously and avoiding trivial solutions.

Random Walker is initialized with a set of voxels taking one of a predefined set of labels. The probability that a random walker starting at a given unlabelled voxel will first reach a voxel of a particular label is computed, based on solving a so-called Dirichlet problem with boundary conditions at the locations of the seed points and the seed point in question fixed to unity while the others are set to zero.

The introduced Random Walker segmentation needs input seeds in order to generate the random walks. We will introduce a method, based on the ellipse fitting method for detecting nuclei, that takes into consideration the points obtained as belonging to the ellipse. The seed points taken into consideration for the Random Walker segmentation are represented by a shrank ellipse. We perform a shrinkage by a factor of two. The remained seed points can be seen in Figure 1(a).

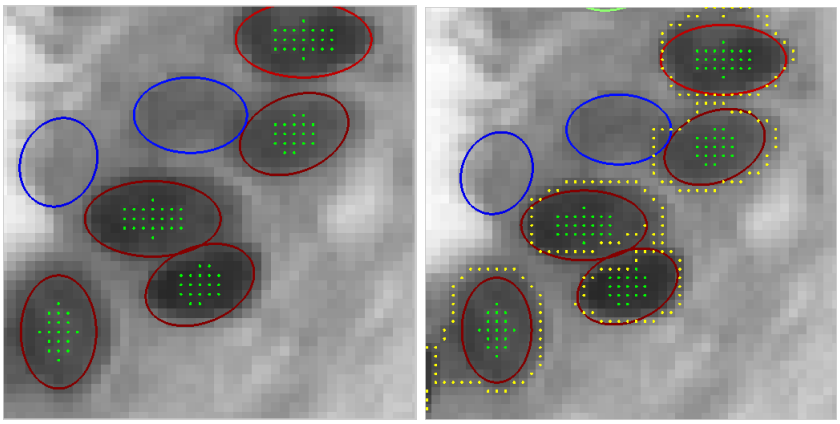

(a) (b)

Figure 1: Random Walker Segmentation(yellow) based on ellipse detection

Segmenting nuclei using the random walker is graphically exemplified in Figure 2. In sub-figure 2(a) the image containing the nucleus to be segmented is extracted. The points belonging to the detected ellipses are plotted in yellow, and will be later considered as seed points for the random walker. In sub-figure 2(b) these points are dilated by a predefined value in order to be included as border value for the random walker segmentation. In this way, an accurate segmentation can be performed to preserve borders of touching or overlapting nuclei. Allowing the random walker algorithm to segment the image taking into consideration the boundary conditions previously defined, the resulting segmentation is displayed in Figure 2 c.

In Figure 1 the ellipses surrounding detected nuclei having a high confidence value are highlighted in red, while the blue ones are considered to be with low confidence. For nuclei segmentation we take into consideration only nuclei having a confidence value above a pre-set threshold value in order to remove outliers. The results can be seen in Figure 1(a), where the blue ellipses are considered as outliers.

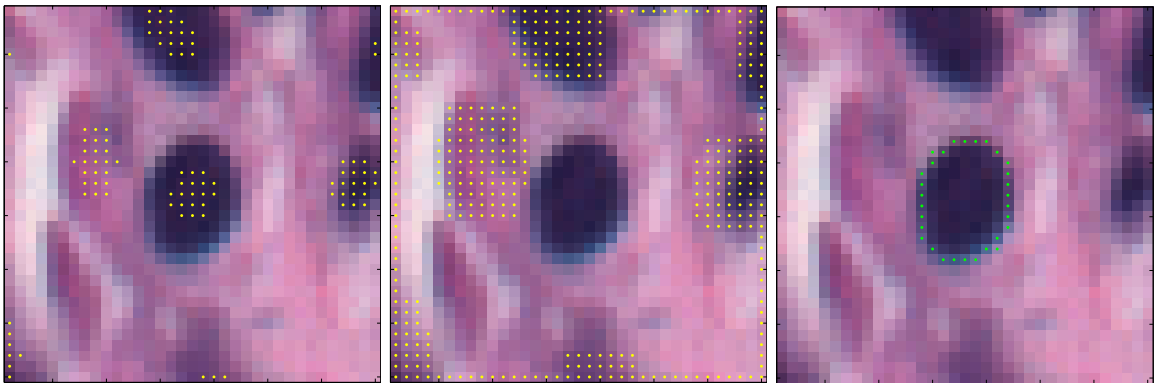

(a) Seed points (b) Dilated Background Seed Points (c) Segmentation Results

Figure 2: Random Walker Segmentation Steps

2.2.1 Hessian Based Features

Based on the information encoded by the Hessian matrix computed at each pixel position, a precise analysis of the anatomical structure it belongs to, can be performed [2]. The eigenvalues of the Hessian matrix are of particular interest as they encode shape information that we further use as feature for classification. By analysing the Hessian matrix at every pixel of the image, a precise analysis can be performed to investigate if the pixel belongs to a blob or to a line structure, as well as if it belongs to a high contrast or to a low contrast region. For 2D structures, the eigenvalues of the Hessian matrix will provide enough information to distinguish between ridge-like and blob-like structures.

Introduced by Frangi et al. [6], the deviation from a blob like structure is defined as the ratio of the eigenvalues of the Hessian Matrix:

$$R_B = \frac{|\lambda_1|}{|\lambda_2|} \tag{1}$$

and the structureness as the measure used in differentiating between foreground and background objects:

$$S = ||H||_F = \sqrt{\lambda_1^2 + \lambda_2^2} \tag{2}$$

Taking into consideration the appearance of nucleus structures in histopathology slides, the method should focus on finding blob-like structures with dark appearance. This translates into positive similar values for the two eigenvalues ($\lambda_1 \approx \lambda_2 \gg 0$) and a high value for the structureness measure. We use a non-max suppression on the image obtained from the ratio of the eigenvalues and then we apply the threshold condition imposed on the Frobenius norm image to identify the nuclei for which these Hessian-based features are computed. We note that the feature R_B should be higher for malignant nuclei and also exhibit a greater variation. We note that Hessian-based features have been used for nuclei detection in Bilgin et al. [2].

2.2.2 Fourier Shape Descriptors

The second category of morphometric features are extracted from Fourier Shape Descriptors, and are based on a precise nuclei detection and segmentation. Since the Fourier Descriptors can encode size and shape information for different geometric shapes, we will extract these descriptors and based on the resulting spectra, we will extract features that distinguish malignant nuclei from benign ones.

A relevant parameter for the Fourier Shape Descriptors is represented by the number of Fourier coefficients. This number must be chosen in such a way to encode a best description of the contour. We perform several tests and a good compromise value for an accurate contour description of the nucleus versus computation burden can be achieved using 10 Fourier Descriptors.

The steps performed in order to compute the Fourier Shape Descriptors, are now introduced:

- *Step 1* Accurate nuclei detection using the Generalized Fast Radial Transform method
- *Step 2* Nucleus boundary segmentation using the Random Walker Segmentation
- *Step 3* Several morphological operations to obtain only the boundary of the nucleus.
- *Step 4* Computing center of masses for the nucleus center coordinates, followed by a computation of euclidean distance from the center to all the boundary points. The angle with respect to the center coordinates is computed and only unique angles associated with distances are taken into consideration.
- *Step 5* Compute the discrete Fourier Transform on the contour points extracted during Step 4, extract the first cosine term corresponding to the average value of the signal(DC component) and the general cosine and sine terms. The Fourier approximation is now complete.

Detecting the irregularity in nuclei shape can be done by analysing the Fourier spectrum in Figure 3. We design the feature extraction method based on small non-DC values for circular nuclei and a high non-DC peak value for the elliptical nucleus presented in sub-figure 3(b). For the irregular nuclei, presented in sub-figure 3 (c), a non-DC peak followed by a smaller non-DC peak at a higher frequency can be observed. The features used by our algorithm will focus on counting the number of irregular nuclei in each image sample, by detecting the second non-DC peak. It is known that a malignant image will have a high number of irregular nuclei, while a benign image will exhibit small irregularities at the shape of nuclei.

2.2.3 Novel Angular Features

The third developed morphometric feature, captures one of the aspects investigated by the pathologists when establishing the degree of malignancy of a histology slide: the orientation of nuclei around ductal structures. A benign sample will have nuclei displaced in a regular arrangement with small variation in size and shape. A uniform pattern of nuclei is considered to be a sign of non-cancerous tissue. For a benign case, the white tissue representing the lumen, is surrounded by epithelium and then by a layer of nuclei, displaced in a parallel way. For a malignant slide, the glands are missing and the nuclei have a high variation in size and shape. The angular nuclei and random orientation observed in malignant images is considered to be a sign of malignancy. The described method will perform a principal component analysis(PCA) on each of the nuclei surrounding glandular structures. The regular pattern around glands will be captured by computing the angle between the principal direction of the nucleus and the normal vector to the gland surface. The method is graphically exemplified in Figure 4(a). A consistent parallel distribution of nuclei will result in a small standard deviation for angles surrounding the gland, but also in small mean angular values.

Since investigating the arrangement of nuclei around ducts and glands requires an accurate gland and nuclei segmentation, in the following, the gland segmentation and nuclei segmentation post processing steps are introduced.

Gland detection and segmentation is based on the segmentation method described in Peng et al. [16]. Using the K-Means algorithm as an unsupervised learning method, we segment the images in four different clusters:

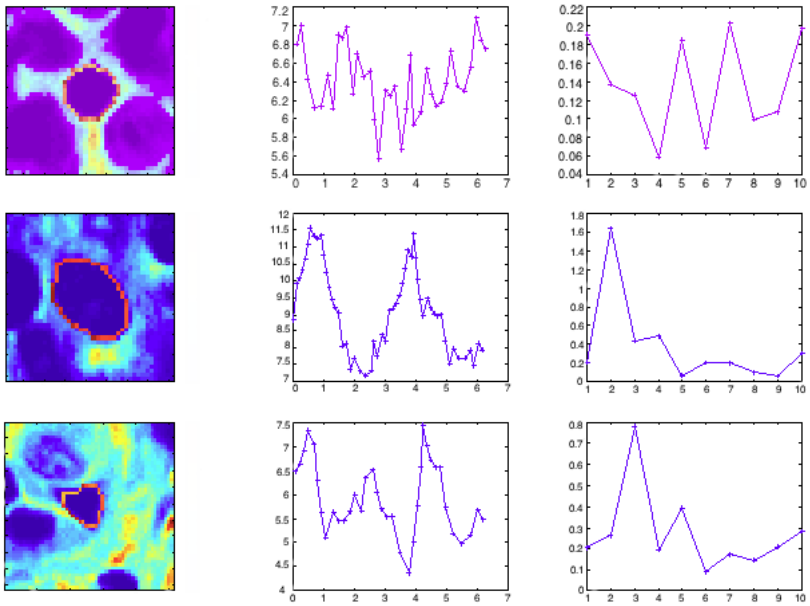

Figure 3: Fourier Descriptors for Different Nuclei Shapes: top row: circular nucleus, middle row: elliptical nucleus, bottom row: irregular nucleus

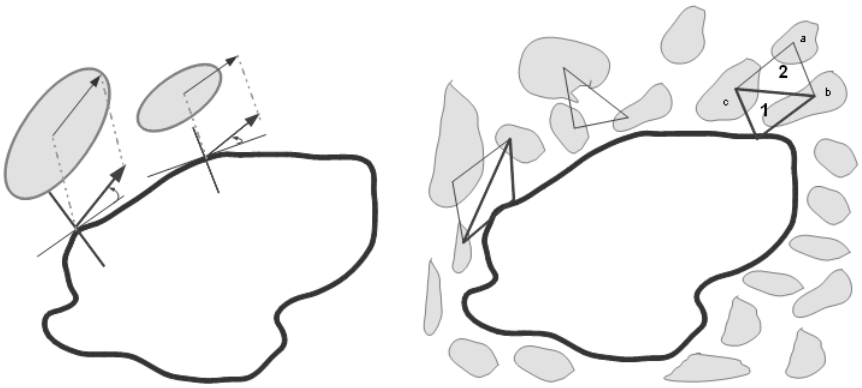

(a) (b)

Figure 4: Nuclei Parallelism(please refer to text for explanation)

glandular lumen, stromal tissue, epithelial-cell cytoplasm and cell nuclei. The K-Means clustering method aims at assigning data into k clusters based on the nearest mean. Since the centroid identification number corresponding to the k clusters is different between images, a consistent assignment must be performed.

Each centroid location returned by the K-means algorithm encodes the R, G and B value corresponding to one of the k tissues. Given the matrix representing the centroid locations as a matrix of 4(tissues) $\times$3(RGB values), the following condition is applied in order to obtain the minimum line index corresponding to the index belonging to the lumen tissue:

$$lumenIndex = \min\left\{\frac{stdC}{meanC}\right\} \tag{3}$$

where $stdC$ is the **Standard Deviation** for a sample x containing n elements: $s = (\frac{1}{n-1}\sum_{i=1}^{n}(x_i - \bar{x})^2)^{\frac{1}{2}}$ and $\bar{x} = \frac{1}{n}\sum_{i=1}^{n} x_i$ is the **Mean Value** for the values belonging to the sample.

Noise removal is performed during the post-processing steps and is done using a mathematical morphological dilation followed by an erosion(closing) operation. A connected components methods is applied in order to separate lumen structures for a further analysis. For each of the resulted structures a series of conditions are applied in order to ensure an accurate gland detection:

- **Condition 1**: A size threshold is applied based on empirical observations in order to reduce too small or too large structures present in the image.
- **Condition 2**: By applying a median filter with a set neighborhood window, the structure should not split into more than n structures. Since gland structures usually have a circular aspect, by applying a median filter with a larger neighborhood value we can discard long and thin lumen structures that separate into many components and don't behave like they do in typical glandular structures.
- **Condition 3**: A gland structure must be surrounded 360° by nuclei. The nuclei segmentation based on Random Walker is used in detecting nuclei surrounding the lumen structure. An empirically selected radius is used for the circular structure centred in the center of masses belonging to the lumen area. The histogram of nuclei surrounding the lumen area is computed and used to represent the distribution of the angles. The selection criteria uses a threshold value to select how many empty bins the histogram can have.

Nuclei post-processing Nuclei shape is representative since we are interested in finding the axis indicating the principal direction. A series of conditions must be enforced to ensure that only relevant structures are kept for further analysis, and will be now introduced:

- **Size Threshold** A removal of structures smaller than an empirically determined threshold is performed to discard small nuclei that will not have a significant impact.
- **Circularity** A removal of nuclei having a perfect circular shape must be performed, since the principal direction will not be an accurate measure for this type of nuclei shape. A principal component analysis is performed on the nuclei shape to find the two eigenvectors and their corresponding eigenvalues. By computing the ratio of these two eigenvalues, a measure of circularity can be further analysed.
- **Irrelevant Nuclei** The introduced angle computation method will take into consideration nuclei in close relation to the glands. The nuclei to be taken into account are those encountered in the close proximity to the gland borders. A distance transform is used to obtain the nuclei in a circular radius around the glandular structure. In order to discard nuclei that are too far away to be relevant, a Delaunay Triangulation is performed. Given the center of masses for each of the nucleus and the points belonging to the lumen surface, a Delaunay triangulation is applied. A closer analysis of the obtained triangles will result in discarding nuclei present in the second row. A nucleus will be removed if it has edges connecting only other nuclei centroids. If there is a direct connection to the lumen surface, the nucleus is kept for further analysis. In Figure 4 all nuclei belonging to triangle 1 have connections to the lumen surface, so their edges will be kept and nucleus b and c will be taken into consideration for future angle computation use. For triangle number 2 all the connecting edges belong to nuclei centroid positions, so the nucleus a, will be removed.

2.3 Texture Features

A texture classification system for automatic differentiation of prostate cancer grades, has been introduced in Khurd et al. [12]. A filtering step followed by clustering is done in order to identify basic texture elements, so called textons. The distribution of these textons provides a discriminative signature for each tumor grade present in prostate cancer, and is used as input for a support vector machine(SVM) classifier.

An adaptation of the framework used for texton generation in prostate cancer is presented in the following: for every image belonging to cancer/non cancer class, an appropriate rotationally invariant filter bank is used to extract responses at each pixel level. We are using a rotationally invariant filter bank presented in Varma and

Zisserman [18]. The Maximum Response(MR) filter bank, consists of a number of filters at multiple orientations, but their output consists of a record computed only at the maximum filter response. The MR8 filter, used in our texton generation, is computed at three scales, giving a total of six responses, three for the edge filter and three for the bar filter. The remaining two filters are the Gaussian Filter and the Laplacian of Gaussian.

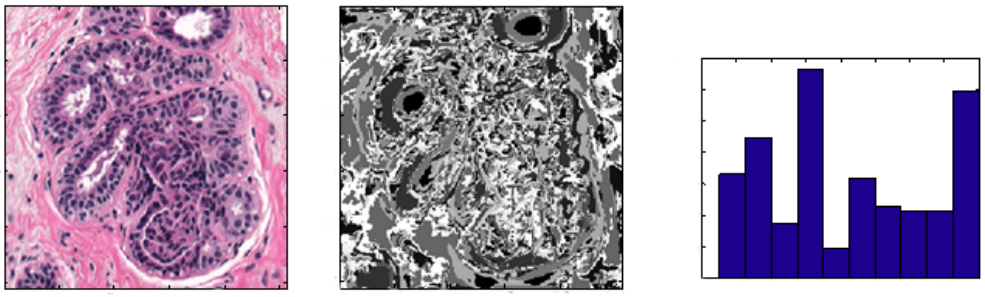

(a) Original Image (b) Texton Map (c) Texton Histogram

Figure 5: Texton Map and Histogram

An accurate description of the texture characteristics can be achieved using the high-dimensional feature space of filter-responses, but a sparser representation preserving the information content is required for the classifier. A clustering technique was performed on the filter response space in order to obtain basic texture elements, or textons, for each texture class. We are using a k-means clustering technique with k clusters for each class. By concatenating the cluster centers obtained from the two classes(malignant and benign), a texton map is created (Figure 5(b)). For each analysed image, the value of each pixel in the texton maps corresponds to the index of the cluster centroid that is closest to the filter response vector at that pixel. The SVM classifier will use as input features the histogram (Figure 5(c)) of each texton map image.

2.4 Network Features

As in many problems in pattern recognition, we are given a set of points in the plane and it is desired to find a structure among these points in the form of edges connecting a subset of the pairs of points. The points we are given are the detected nuclei in the histopathology images, previously detected using the ellipse radial symmetry and the edges we are interested in are the ones surrounding structures presenting interest for the pathologists. We are using an approximation of the relative neighborhood graph, respectively the Urquhart graph[1], as it provides fast computation and good human matching perspective of the shape of the set. Since different studies showed the importance of cell nuclei belonging to the same anatomical structure [2], we take into consideration the distribution of the stromal tissue and we perform a segmentation of the extracellular matrix. Based on this approach we do a separation of stromal tissue. Performing the separation of stromal/non-stromal tissue is being done by applying the K-means algorithm using 4 classes (glandular lumen, stroma, and epithelial-cell cytoplasm and cell nuclei), followed by an extraction of the non-stromal tissue. Post-processing by spatial smoothing is done using the Random Walker algorithm [7]. The random walker prior probabilities are obtained by fitting a Gaussian mixture model to the K-means clusters. We are able to perform an improved separation of structures and a more representative network computation that takes into consideration different structures present in the sample.

By taking into consideration the extracellular matrix and using the Urquhart graphs, the network cycles used in Khurd et al. [13] are employed in extracting network statistics designed to capture cancer specific hallmarks. We compute the weighted and unweighted lengths of different cycles, as well as various statistics: number of cycles with length greater than 3, average non-triangular cycle length and maximum non-triangular cycle length. We have also used various network features that could capture the specific pattern of cancer cells in the malignant tissue [9]: number of vertices, number of graph components, clustering coefficients, Fiedler values computed from the vertex Laplacian and the edge Laplacian and average shortest path length.

2.5 Feature Selection

Feature selection is the technique of selecting a subset of relevant features for building robust learning methods by reducing the training complexity and increasing the accuracy. As currently used databases contain more and more features, the majority of which is often redundant or irrelevant, the necessity of selecting relevant features arises. A feature selection method should improve the prediction performance of the classifier while providing a faster and more cost-effective classification system. It has to produce simpler classification models and gain an insight in the underlying process that generated the data.

Because a simple combination of features that provide a high classification performance doesn′t necessarily provide a better feature set[11], different methods that take into consideration the dependency among features (redundancy) have been developed by Peng et al. [15] and by Yu and Liu [19].

The minimum redundancy-maximum relevance feature selection is a robust and accurate feature selection technique that extracts features minimally redundant among themselves and maximally relevant to the target classes.

Maximum Relevance: is a feature selection criterion which approximates $\mathbf{J}(\mathbf{S_m}, \mathbf{c})$ in equation with the mean value of all mutual information values between individual feature x_i and class c:

$$\max\ D(S,c)\ ,\ \ \mathbf{D}=\frac{\mathbf{1}}{|\mathbf{S}|}\sum_{\mathbf{x_i}\in\mathbf{S}}\mathbf{I}(\mathbf{x_i};\mathbf{c}) \tag{4}$$

where $\mathbf{I}$ is the mutual information and $|\mathbf{S}|$ is the number of features in S. Since the remained features might have a high redundancy property another feature selection must be performed after applying the maximum relevance criterion.

Minimal Redundancy: is a feature selection criterion that selects mutually exclusive features:

$$min\ R(S)\ ,\quad R=\frac{\mathbf{1}}{|\mathbf{S}|^{\mathbf{2}}}\sum_{\mathbf{x_i},\mathbf{x_j}\in\mathbf{S}}\mathbf{I}(\mathbf{x_i};\mathbf{x_j}) \tag{5}$$

The MRMR method finds the subset of features that maximizes D-R in an incremental manner by adding one feature at a time.

3. RESULTS

In this section we show the details of the experiments on both texton features and network features used. Experiments are based on 512×512 image patches that were taken from large, several GPixel large, $H\&E$ stained "virtual slides". For the texton analysis the results are computed using images down-sampled by a factor of 2. The slides are sampled at 0.47 microns/pixel, corresponding to $40X$ objective scan. A number of 100 patches were marked by pathologists as "diagnostically relevant" and labelled as malignant or benign. For training the support vector machine(SVM) classifier we selected 30 images(15 of each type: malignant and benign) and for validation of our algorithm the rest of 70 images had been used. We perform 10 runs for different train/test partitions and report mean and standard deviation values of the classification accuracies and the area under the ROC (Receiver Operating Characteristic) curve. The reported classification results are obtained using the LibSVM library for support vector machines [4]. We have used a radial basis kernel $K(x_i, x_j) = exp(-\gamma||x_i - x_j||^2$, with $\gamma = \frac{1}{number\ of\ features}$.

Morphometric Features

The set of morphometric features is captured from the nuclei size based on the Random Walker Segmentation, the Fourier Shape Descriptors, and from the computation of the Hessian matrix for every pixel in the image.

The nuclear size is computed by finding the number pixels belonging to each segmented nucleus. The random walker segmentation is applied on the original image data-set, pre-processed by extracting only the H channel. Computing the standard deviation of the nuclear size over each of the images from the data-set will capture this

relevant cancer specific mark. A good feature used in distinguishing between malignant and benign samples is the mean value of the R_b defined in the methods section computed over the entire image.

Detecting the irregularity in nuclei shape can be done by analysing the Fourier spectrum in Figure 3. It can be noticed that all non-DC values for circular nuclei are quite small, while for the elliptical nucleus presented in sub-figure 3(b), there is only one non-DC peak value. For the irregular nuclei, presented in sub-figure 3 (c), a non-DC peak followed by a smaller non-DC peak at a higher frequency can be observed. The features used by our algorithm will focus on counting the number of irregular nuclei, by detecting the second non-DC peak. We consider the first peak to occur at a value of 0.15 of the maximum energy value and the second one at 0.05. It is considered that a malignant image will have a high number of irregular nuclei, while a benign image will exhibit small irregularities at the shape of nuclei. The feature taken into consideration is the number of irregular nuclei in each sample.

Table 1: Results of Classification using Morphometric Features

Testing Details	*Benign Class Accuracy*	*Malignant Class Accuracy*	*Area Under the Curve*	*Classification Accuracy*
Mean Ratio of Eigenvalues of Hessian Matrix	66.29±14.11	69.14±18.26	0.72±0.08	67.71±4.27
Standard Deviation in Nuclei Size	83.71±6.87	66.29±11.49	0.81±0.02	75.00±4.00
Mean of the Angular Feature	68.29±5.63	62.57±3.42	0.65±0.05	65.43±3.07
Irregular Number of Nuclei (Fourier Shape Descriptors)	57.43±10.03	54.00±9.57	0.55±0.05	55.71±4.57

Textural features: We perform a K-means algorithm using 43000 randomly chosen pixels in each of the 15 images belonging to one class and we obtain 11 centers, resulting in a total of 22 concatenated cluster centers from both classes. We then compute the texton maps and a 22 bin histogram for each of the 30 images for the train partition and 70 images for the test partition.

We have conducted tests on the provided data-set using a different pre-processing step. In first instance all three channels (R,G,B) and filtered using the filter bank and the resulting texton histogram is obtained from a 3(image channels) $\times$8 (filter bank) stack of images(row 1 in Table 2). Based on the color transform previously introduces, a texton map adding up the two channels is computed. Using only one 1×8 image stack, a grayscale, red channel and H channel texon histograms are performed. In Table 2, the classification results are presented. We notice that the textons computed on the H channel of the pre-processed image provide best classification accuracy.

Table 2: Results of Classification using Textons

Testing Details	*Benign Class Accuracy*	*Malignant Class Accuracy*	*Area Under the Curve*	*Classification Accuracy*
RGB Textons	80.00±7.62	72.57±9.06	0.8204±0.0464	76.29±2.95
H & E Textons	76.29±7.74	76.29±9.24	0.8433±0.0274	76.29±3.45
Grayscale Textons	80.57±10.76	73.71±8.17	0.8449±0.0260	77.14±3.87
Red Textons	81.71±10.71	77.71±9.31	0.8779±0.0345	79.71±3.68
H Textons	83.71±6.03	78.29±12.72	0.8801±0.0350	81.00±6.53

Network features: We take into consideration the network cycle features introduced in Khurd et al. [13] that take advantage of cycle structure present within the cell networks, created using different networks. The network cycles are extracted using the face-tracing algorithm presented in Gross and Yellen [10], and a removal

of all long Delaunay edges with Euclidean length above a cut-off value σ is performed. Given different cycles, we compute their unweighted and weighted lengths(with weights based upon the Euclidean distance) and then compute various statistics: number of cycles with length greater than 3, average non-triangular cycle length and maximum non-triangular cycle length. Additional features are computed, among which are the edge Laplacian, Fiedler Value, Kirchoff index, Wiener index, according to Grady and Polimeni [9]. We have used a network parameter variation to obtain the best classification results, based on different types of networks and features. For network creation we have used Urquhart graphs, K-nearest neighbor graphs, epsilon-nearest neighbor and Delaunay Triangulation. The average shortest path between nuclei is the best feature and gives performance comparable to the textons for 10 train/test partitions.

Table 3: Results of Classification using Network Statistics

Testing Details	*Benign Class Accuracy*	*Malignant Class Accuracy*	*Area Under the Curve*	*Classification Accuracy*
Mean Cycle Weighted Euclidean Length	58.86±13.81	76.57±12.83	0.71±0.04	67.71±6.40
Number of Connected Components	57.43±3.68	88.57±4.26	0.73±0.04	73.00±1.84
Average shortest path between nuclei	70.00±8.75	90.86±4.43	0.87±0.01	80.43±3.16

Combining Features for Optimal Results

We wish to investigate the discriminatory power of combining different features capturing individual hallmarks of cancer. We developed features that take into consideration the special arrangement of nuclei, the size and shape variation properties but also special texture analysis.

The set of final features contains 1 network cycle feature (mean cycle weighted euclidean length), 2 network features (average shortest path between nuclei and number of connected components in the graph), 2 morphometric features (mean size of nuclei and mean value for the ratio between the eigenvalues of the Hessian matrix) and 22 texton features computed on the H channel(histogram for each class contains 11 bins), summing up to a 27-dimensional feature set.

Table 4: Classification using MR-MR Feature Selection

Testing Details	*Benign Class Accuracy*	*Malignant Class Accuracy*	*Area Under the Curve*	*Classification Accuracy*
No Feature Selection	87.14±7.74	87.81±8.94	0.94±0.02	86.43±4.73
With Feature Selection(18 features)	86.57±14.11	87.71±8.94	0.94±0.02	87.14±4.31
With Feature Selection(10 features)	84.86±9.53	89.14±8.06	0.93±0.02	87.00±3.72
With Feature Selection(8 features)	85.71±9.04	88.29±7.67	0.93±0.02	87.00±2.56
With Feature Selection(7 features)	84.86±8.52	86.57±8.52	0.93±0.02	85.71±2.52

Effect of image compression on classification performance:

We used $JPEG2000$ to compress the 100 images at different levels (8, 16, 32, 64, 128) and re-computed the classification performance of our integrated system (again with 18 features selected using MRMR). The performance is plotted in Fig. 6(a), (b) and Table 5. Our system was extremely robust with respect to compression.

It is not surprising that the network features are nearly invariant w.r.t. compression since they only depend upon nuclei locations. Despite severe degradation in the compressed images, we additionally observed that the re-computed texton and morphometric features are also quite robust to image compression.

Table 5: Results of Classification using Different Compression Levels

Compression level	*Benign Class Accuracy*	*Malignant Class Accuracy*	*Area Under the Curve*	*Classification Accuracy*
Original data set uncompressed	86.57±7.74	87.71±8.94	0.9385±0.0249	87.14±4.31
8	86.86±6.89	86.57±6.32	0.9265±0.0312	86.71±2.94
16	88.29±6.09	84.86±9.99	0.9342±0.0321	86.57±4.43
32	86.57±8.20	84.86±9.90	0.9375±0.0325	85.71±4.31
64	86.00±6.52	87.14±8.75	0.9398±0.0239	86.57±3.10
128	86.29±8.06	85.14±10.06	0.9327±0.0331	85.71±3.69

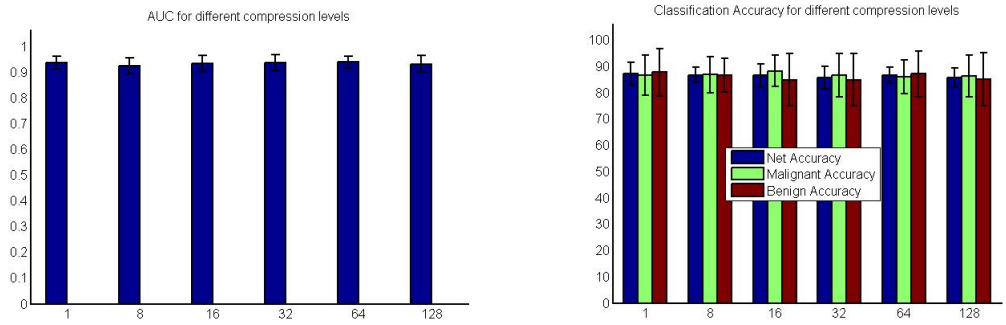

(a) (b)

Figure 6: Classification Results using Compression

4. DISCUSSION AND CONCLUSION

The results presented in Table 4 summarize our experimental trials. Given the 27-dimensional set of features the classification accuracy combining textural features, network features and morphometric features reaches 86.43 ± 4.73. We note that individual features achieve an inferior best classification accuracy: 80.43 ± 3.16 for the feature encoding the average shortest path between nuclei and 81.00 ± 6.53 for the textons based on H channel from pre-processed images. Combining these texton features, network features and features encoding nuclei statistics proves an advantage over individual method classification. This is because the complementary information provided by the different individual features captures different cancer manifestations in breast histopathology

The Maximum Relevance - Minimum Redundancy(MR-MR) method used for feature selection, proves it's usefulness. In Table 4 the second row provides the best classification accuracy obtained using the feature set previously introduced. It can be seen that by using the mutual information to measure the statistical dependency between features, the minimum redundancy-maximum relevance feature selection extracts features minimally redundant among themselves and maximally relevant to the target classes. One of the parameters required by the MR-MR is the number of best independent features to be taken into consideration. We observe that by using only 8 features out of a total of 27 the accuracy is boosted from 86.43 ± 4.73 to a value of 87.00 ± 3.72. Adding more features to the data set used for classification saturates the classification accuracy since the features are not exhibiting any more orthogonal properties. Analysing which of the 8 features taken into consideration for the MR-MR feature selection, reveals a combination of network features, texton features and morphometric features. In each of the 10 runs performed, the average selection for the features is composed of 4 to 5 most discriminatory textons followed by a best ranking of the network features combined with morphometric features.

In future work, we plan to develop novel morphometric features obtained by clustering the Fourier shape spectra to identify different classes of normal and abnormal nuclei. We also plan to investigate the effects of image compression on classification accuracy results and assess the usefulness of our system compared to clinicians inter-rater variability.

ACKNOWLEDGMENTS

This work was supported by National Institutes of Health/National Institute of Biomedical Imaging and Bioengineering (NIH/NIBIB) under Grant R01EB008055.

References

[1] D.V. Andrade and L. De Figueiredo. Good approximations for the relative neighbourhood graph. In *Proceedings of the 13th Canadian Conference on Computational Geometry (CCCG01)*, pages 25–28, 2001.

[2] C.C. Bilgin, P. Bullough, G.E. Plopper, and B. Yener. ECM-aware cell-graph mining for bone tissue modeling and classification. *Data mining and knowledge discovery*, 20(3):416–438, 2010.

[3] HJG Bloom and WW Richardson. Histological grading and prognosis in breast cancer: a study of 1409 cases of which 359 have been followed for 15 years. *British Journal of Cancer*, 11(3):359, 1957.

[4] Chih-Chung Chang and Chih-Jen Lin. LIBSVM: A library for support vector machines. *ACM Transactions on Intelligent Systems and Technology*, 2:27:1–27:27, 2011. Software available at http://www.csie.ntu.edu.tw/ cjlin/libsvm.

[5] E. Cosatto, M. Miller, H.P. Graf, and J.S. Meyer. Grading nuclear pleomorphism on histological micrographs. In *Pattern Recognition, 2008. ICPR 2008. 19th International Conference on*, pages 1–4. IEEE, 2008.

[6] A. Frangi, W. Niessen, K. Vincken, and M. Viergever. Multiscale vessel enhancement filtering. *Medical Image Computing and Computer-Assisted Interventation MICCAI 1998*, pages 130–137, 1998.

[7] L. Grady. Multilabel random walker image segmentation using prior models. In *Computer Vision and Pattern Recognition, 2005. CVPR 2005. IEEE Computer Society Conference on*, volume 1, pages 763–770. IEEE, 2005.

[8] L. Grady. Random walks for image segmentation. *IEEE transactions on pattern analysis and machine intelligence*, pages 1768–1783, 2006.

[9] L.J. Grady and J.R. Polimeni. *Discrete Calculus: Applied Analysis on Graphs for Computational Science*, volume 3. SpringerLinkLink, 2010.

[10] J.L. Gross and J. Yellen. *Graph theory and its applications*. CRC press, 2006.

[11] J. Jäger, R. Sengupta, and W.L. Ruzzo. Improved gene selection for classification of microarrays. In *Proceedings of the eighth Pacific Symposium on Biocomputing: 3–7 January 2003; Lihue, Hawaii*, pages 53–64, 2003.

[12] P. Khurd, C. Bahlmann, P. Maday, A. Kamen, S. Gibbs-Strauss, E.M. Genega, and J.V. Frangioni. Computer-aided gleason grading of prostate cancer histopathological images using texton forests. In *Biomedical Imaging: From Nano to Macro, 2010 IEEE International Symposium on*, pages 636–639. IEEE, 2010.

[13] P. Khurd, L. Grady, A. Kamen, S. Gibbs-Strauss, E.M. Genega, and J.V. Frangioni. Network cycle features: Application to computer-aided gleason grading of prostate cancer histopathological images. In *Biomedical Imaging: From Nano to Macro, 2011 IEEE International Symposium on*, pages 1632–1636. IEEE, 2011.

[14] G. Loy and A. Zelinsky. A fast radial symmetry transform for detecting points of interest. *Computer Vision-ECCV 2002*, pages 358–368, 2002.

[15] H. Peng, F. Long, and C. Ding. Feature selection based on mutual information criteria of max-dependency, max-relevance, and min-redundancy. *Pattern Analysis and Machine Intelligence, IEEE Transactions on*, 27 (8):1226–1238, 2005.

[16] Y. Peng, Y. Jiang, L. Eisengart, M.A. Healy, F.H. Straus, and X.J. Yang. Segmentation of prostatic glands in histology images. In *Biomedical Imaging: From Nano to Macro, 2011 IEEE International Symposium on*, pages 2091–2094. IEEE, 2011.

[17] M. Singh, J. Ni, and C. Bahlmann. Generalized fast radial symmetry transform (GFRS) for ellipse detection and application to histopathology for ellipse detection and application to histopathology, Siemens Internal Technical Report, SCR-12-TR-880, 2011.

[18] M. Varma and A. Zisserman. Classifying images of materials: Achieving viewpoint and illumination independence. *Computer Vision-ECCV 2002*, pages 255–271, 2002.

[19] L. Yu and H. Liu. Efficiently handling feature redundancy in high-dimensional data. In *Proceedings of the ninth ACM SIGKDD international conference on Knowledge discovery and data mining*, pages 685–690. ACM, 2003.